DOI: 10.2352/ISSN.2470-1173.2016.12.IMSE-280

Characterization of VNIR Hyperspectral Sensors with Monolithically Integrated Optical Filters

Prashant Agrawal[1], Klaas Tack[1], Bert Geelen[1], Bart Masschelein[1], Pablo Mateo Aranda Moran[2], Andy Lambrechts[1], Murali Jayapala[1]; [1]Imec vzw., Leuven B-3001 Belgium; [2]TMC Zaventum B-1935 Belgium

Abstract

Imec has developed compact hyperspectral image sensors where optical filters are monolithically integrated over standard off-the-shelf CMOS image sensors. These filters are implemented at individual pixel level and are Fabry-Perot interferometers. Due to the monolithic integration of optical filters on the image sensors, the characterization procedures and camera response model developed for traditional sensors cannot be directly used for these hyperspectral sensors. In this paper, we present the procedures used for characterizing these sensors and deriving a suitable camera response model for them.

Introduction

Sensor characterization and camera response modeling are important for system configuration exploration, performance analysis, system benchmarking, stress testing and design space exploration. The hyperspectral image sensors developed by imec are based on optical filters, monolithically integrated over standard off-the-shelf CMOS image sensors [1]. This approach enables design of hyperspectral sensors where the filter pattern, spectral range, spatial resolution per filter and the filter responses can be customized based on end application requirements. These sensors are unique as a large number of optical filters can be monolithically integrated at a pixel level on CMOS sensors with pixel sizes as small as 2µm. The characterization procedures and camera models for these sensors are not well defined and, to the best of our knowledge, are not available in the current state of art. It is also not straightforward to determine if the procedures and models for traditional sensors can be used for these hyperspectral sensors. Our work focuses on exploring the current procedures and models, and suitably optimizing and adapting them for these hyperspectral sensors.

In this paper, we present a camera response model for these hyperspectral sensors. The traditional camera response model has been adapted to take into account the dependence of filter response of these sensors on the angle of incident light. We also present approaches for noise and dark current measurement for these hyperspectral sensors. As mentioned above, imec's approach of monolithically integrating the optical filters on standard-of-the-shelf CMOS image sensors is unique. Hence, the camera response models, noise models and characterization procedures for these sensors are not well defined. To the best of our knowledge, they do not exist in the current state of art. Our work is the first attempt in this direction.

Background

The principle of Fabry-Perot interferometer is illustrated in Figure 1. A Fabry-Perot interferometer consists of two reflecting surfaces with a cavity in between. The incident light undergoes multiple reflections. At each reflection, a part of the light is transmitted which undergoes a constructive interference if the path difference between multiple reflections is an integral multiple of λ (the wavelength of the incident light).

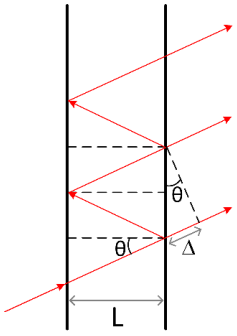

Figure 1 Illustration of the principle of Fabry-Perot interferometer

$$\Delta = 2nLcos\theta = m\lambda \quad (1)$$

where, λ is the central wavelength, m is the harmonic order, n is the refractive index of the material in the cavity between the two surfaces, L is the length between the two surfaces and θ is the Angle Of Incidence (AOI) of the incoming light.

Imec's optical filter design is based on the Fabry-Perot interferometer structure such that filters with specific transmission wavelength are designed by tuning the cavity length (L). Figure 2 shows an illustration of these filters integrated monolithically on standard CMOS image sensors. The cavity length determines the central wavelength of the optical filter and the reflectivity of the two surfaces determines the Full Width Half Max (FWHM) of the filter. These filters can be integrated at per-pixel level, pixel row level and pixel area level to create mosaic [2], linescan [1] and tile [3] patterned hyperspectral sensors, respectively.

As these optical filters are Fabry-Perot interferometers and monolithically integrated on the pixels, the response of these sensor pixels is a function multiple parameters such as (a) wavelength, (b) pixel-position-dependent filter properties such as cavity height and filter materials, and (c) light's AOI, as shown in Equation 1. In Figure 3, we show the impact of different lens aperture on one of the optical filters of an imec hyperspectral sensor. The widening of the lens aperture leads to a shift in the peak wavelength, reduction in the transmission efficiency and increase in the FWHM. This leads to a trade-off between spectral performance of the filters and the sensitivity and speed of the system (determined by the amount of

DOI: 10.2352/ISSN.2470-1173.2016.12.IMSE-280

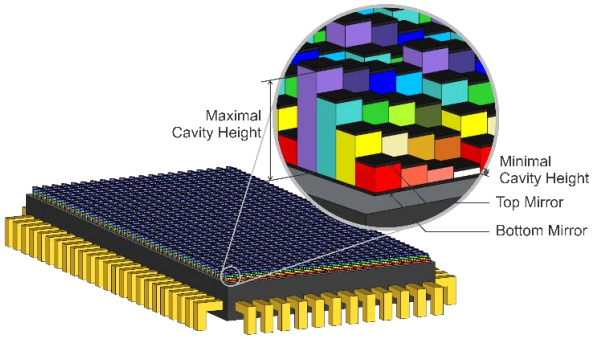

Figure 2 A schematic representation of monolithic integration of Fabry-Perot filter on standard CMOS imager in a pixel-level mosaic pattern [2]

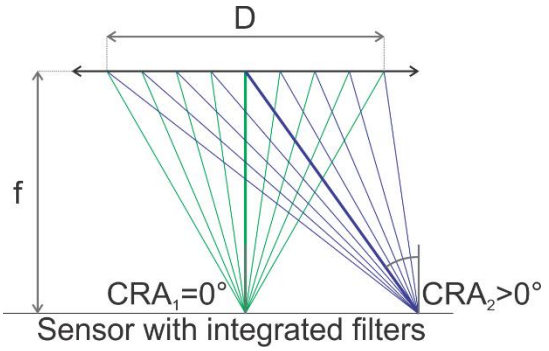

Figure 4 Illustration of the variation in the Chief Ray Angle (CRA) of the light incident at different pixel positions of the sensor

incident light). The optical filters for imec's hyperspectral sensors are designed for high spectral resolution and the number of bands on a single sensor ranges from 16 to 150. Thus, controlling the AOI is critical and it makes it important to take the angle dependence into account in the camera response model for these hyperspectral sensors.

The impact of AOI on the filter's spectral response may be simulated using thin film simulation [4]. In practice, a real world sensor is not illuminated by one discrete AOI, but by a range of angles as determined by the applied lens system (see Figure 3). At the center of the optical axis the sensor and filter are illuminated by a perpendicular cone of light, as determined by the lens' F/# (focal length f over aperture D). Further away from the optical axis, the incident cones of light might be tilted depending on the exit pupil position. This tilting is represented by the pixel-position-dependent Chief Ray Angle of a cone, which is the tilt angle of the central ray of the cone. By integrating over the range of angles determined by the F/# and CRA, the spectral responses across the sensor may be computed.

The direct post-processing of the optical filters on top of an active image sensor is carried out using CMOS compatible processes and

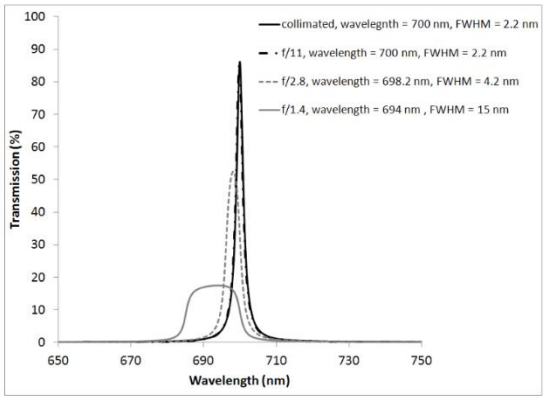

Figure 3 Illustration of the variation in the Chief Ray Angle (CRA) of the light incident at different pixel positions of the sensor

materials such that the functionality of the underlying CMOS image sensor is not affected. [1] provides a good overview of the different filter implementation options and processing constraints. Since it is ensured that the monolithic integration does not impact the characteristic of the underlying CMOS image sensor, parameters such as noise and dark current will not be impacted. However, it is still crucial to be able to measure these parameters for these hyperspectral sensors and verify. Thus, in this work we focus on characterizing and modeling the following relevant sensor parameters – (a) pixel response, (b) noise behavior and (c) dark current.

Pixel Response Model

The response of a pixel is traditionally modeled as shown in Equation 2, where each color channel is considered separately [5]

$$DN_i = k.I \int_{\lambda_1}^{\lambda_N} QE_i(\lambda).F_i(\lambda).O(\lambda).R(\lambda).\emptyset(\lambda)\,d\lambda + \Delta_i \quad (2)$$

where, DN_i is the digital number obtained for a pixel of the i^{th} color channel, k is the conversion gain, I is the integration time, λ is the wavelength of incoming light, $QE_i(\lambda)$ is the quantum efficiency of i^{th} color channel, $F_i(\lambda)$ is the transmittance of the i^{th} color channel of the color filter array, $O(\lambda)$ is the transmission efficiency of the optics (lens, rejection filters, etc), $R(\lambda)$ is the reflectance of the scene, $\emptyset(\lambda)$ is illumination of the scene and Δ_i is a normal random variable denoting noise.

As seen from Equation 2, the model takes into account only the intensity and the wavelength of the light incident on the sensor pixel. However it has been discussed earlier that in imec's hyperspectral sensors, the response of these filters is a function of pixel position as well as the wavelength and AOI of the incident light. To take into account the angular dependency of the incident light, we propose a pixel response model for the hyperspectral sensors, as shown in Equation 3. This model has been adapted from the traditional pixel response model (shown in Equation 2)

$$DN_i = k.I \int_{\lambda_1}^{\lambda_N} \widehat{QE_i}(\lambda,\theta).\widehat{F_i}(\lambda,\theta).O(\lambda).R(\lambda).\emptyset(\lambda)\,d\lambda + \Delta_i \quad (3)$$

where, i denotes an optical filter, θ is the angular distribution of incoming light, $\widehat{QE_i}(\lambda,\theta)$ is the quantum efficiency and $\widehat{F_i}(\lambda,\theta)$ is

DOI: 10.2352/ISSN.2470-1173.2016.12.IMSE-280

the transmittance of the i^{th} optical filter. The remaining terms are similar to as in Equation 2. The hyperspectral sensor has a number of optical filters which have been designed for specific central wavelengths by tuning the cavity height and the cavity material. In this paper, we focus on modeling and measuring the dependence of pixel response on λ and pixel position at *'reference condition'* where $\theta = 0$ (discussed further in next section). We are currently working on developing a procedure for measuring the impact of θ on the pixel response.

QE Measurement

At imec, we have developed a procedure and a setup to carry out QE measurement for each sensor produced so that the impact of any processing variability on the filter responses is accounted for. The QE measurement is also supplied along with other calibration information for each sensor such that it can be used along with the proposed pixel response model (Equation 3) to estimate one or more parameters such as reflectance, optical system response, etc. and to carry out system level exploration.

As the optical filters are monolithically integrated on the CMOS image sensor, it is difficult to measure the response of the filters and the pixels separately. Hence, in our procedure we carry out a combined QE measurement of the filters and the pixel. Thus, we measure $\widehat{QE}_i(\lambda,\theta).\widehat{F}_i(\lambda,\theta)$ together (from Equation 3). The combined QE of the spectral filter and the underlying sensor pixel is measured for each pixel for wavelengths between 400-1000nm (VNIR spectral range).

For optimal QE measurement, the sensors are characterized without any optics. The sensor is illuminated using a reflecting collimator so that the light is incident perpendicularly on the sensor, i.e. AOI=0° (see Figure 5 and Figure 6) which we consider as the *'reference condition'*. We have discussed earlier that AOI of the incident light impacts the spectral performance of the filter. However, from Figure 3, it can be seen that these filters have tolerance to a certain extent towards deviation from the *'reference condition'*. To achieve a good trade-off between the spectral performance of the filters and the sensitivity and the speed of the system, we recommend a maximum lens aperture of f/2.8 for these sensors. Any further deviation from the reference or recommended condition will require that the QE measurements are carried out under those conditions.

A picture of the complete measurement setup is shown in Figure 5. The setup consists of four subsystems. The first subsystem consists of an illuminator (250W Tungsten-halogen lamp) and a monochromator (Acton SP2555 from Princeton Instruments). The illuminator-monochromator subsystem is optimized such that the illuminator output is focused and matched to the monochromator. The illuminator coupling to the monochromator is fixed by mounting the illumination source directly on the monochromator.

The second subsystem is the system that transfers the light from the monochromator to the sensor (Figure 6). A custom designed fiber optic connects the output of the monochromator with the input of a reflective collimator (Thorlabs RC12SMA-P01). The collimator enables the control of the angle of incidence of the light emitted on the sensor.

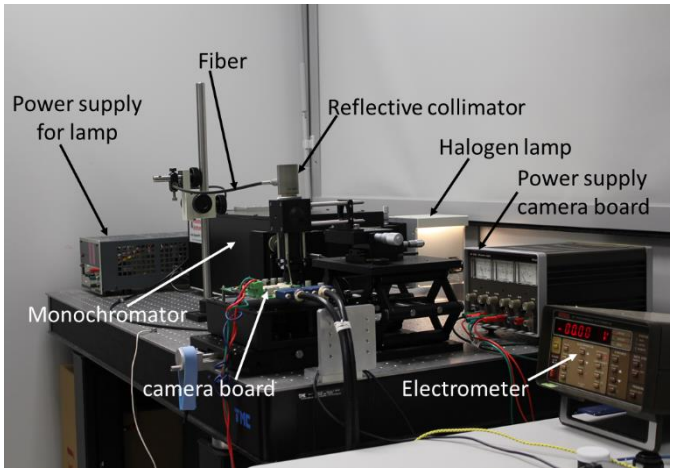

Figure 5 QE measurement setup

The third subsystem is used to calibrate the light source. It consists of a photodiode (Newport 818-UV) interfaced to a programmable electrometer. This reference photodiode is used to measure the number of photons projected on the sensor and is needed to calculate the QE of the sensor.

The fourth subsystem is used to read out the sensor. The sensor under test is mounted on a camera development kit with a cameralink interface to communicate with the test software running on the PC. A combination of x-y-z translation stages are used to align the tested sensor under the collimator such that the sensor is centered and uniformly illuminated. The photodiode is also mounted under the collimator to calibrate the light source. We have developed in-house the software that controls all the sub-systems, acquires data from the sensor and photodiode during calibration and carries out further analysis to calculate the QE.

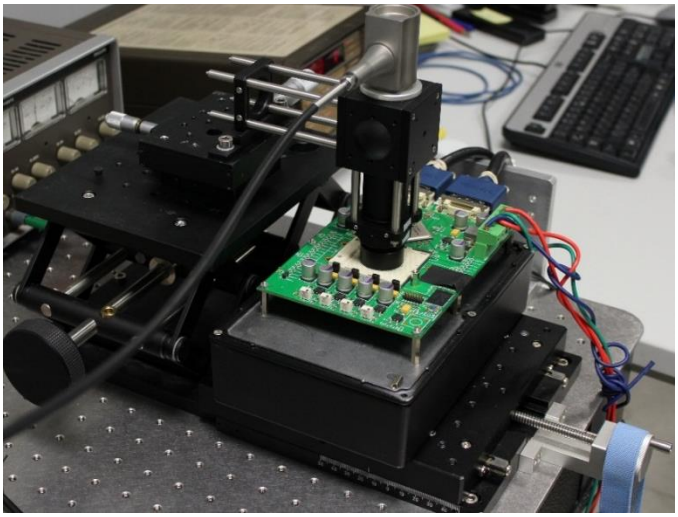

Figure 6 Illumination path from reflective collimator to sensor. The reflective collimator ensures that the light on the sensor is incident perpendicularly and CRA is minimized

DOI: 10.2352/ISSN.2470-1173.2016.12.IMSE-280

The QE measurement procedure consists of the following steps:

1. The monochromator light beam output is calibrated using the reference photodiode where the light power at each wavelength step (used to calibrate the sensor) is measured.

2. A panchromatic image sensor (CMOS image sensor without the monolithically integrated optical filter and referred to as reference sensor here) is calibrated to measure the spatial non-uniformity of the light source. Although the setup is optimized to minimize the non-uniformity of the illumination on the sensor under test, we carry this step to account for any non-uniformity which can be caused by the typical Gaussian fall-off characteristics of the output beam of the collimator.

   The reference sensor is first initialized using a procedure such that the gain and the black level offset of the sensor are optimally set. Images are acquired from the sensor for all wavelengths between 400-1000nm (VNIR spectral range) at steps of 1nm. At each wavelength, the image is acquired using an integration time such that dynamic range is maximized. Dark image is also acquired at the same integration time and it is subtracted from the earlier image for fixed pattern noise removal. QE is calculated for each pixel at each wavelength step. Thus, a three-dimensional hyperspectral cube is obtained for the entire sensor containing $QE_{i,j,\lambda}$ where *(i,j)* is the pixel position and λ is the wavelength step.

3. The three-dimensional hypercube containing QE measurement at each pixel position at different wavelength steps is obtained for the hyperspectral sensor under test in a manner similar to the reference sensor (as described above).

   We compensate for any spatial non-uniformity in the illumination by using the calibration data obtained for the reference sensor in step 2. A ratio of the measured QE at each pixel position and that of a reference QE (measured using a traditional QE measurement setup) is calculated. The variation in the obtained ratio across the pixels gives a measure of the spatial non-uniformity introduced by the illumination. This ratio is then multiplied to the measured QE of the hyperspectral sensor to compensate for the non-uniformities.

4. The pixel level QE measurements after the non-uniformity compensation is used to calculate average response for the pixels corresponding to a particular optical filter. Thus, the average response for all the optical filters implemented on the sensor is calculated and the corresponding central wavelengths and FWHM (Full-Width Half Maximum) are also calculated.

Results

In this section, we will first present results related to the testing of the QE measurement setup and procedure. We will then show the validity of the proposed pixel response model.

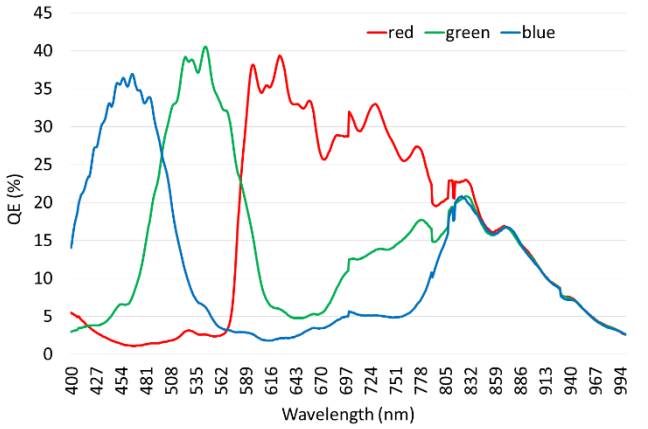

Figure 7 QE measurement of a CMV2000 RGB sensor

For testing the QE measurement, we calibrated a standard CMOSIS CMV2000 RGB sensor. The measured QE (Figure 7) showed a very good match to the reference QE (Figure 8) for the sensor as provided by CMOSIS.

In Figure 9, we show the QE measurement results for one of imec's linescan hyperspectral sensors with 128 bands. This measurement was carried out at reference condition where CRA of the light incident on the sensor was 0 degrees. Similarly, QE measurements were carried out for other imec hyperspectral sensors with tiled and mosaic filter patterns.

In Figure 10, we show the central wavelength for the optical filters at each pixel across the sensor. The central wavelength is calculated using the obtained QE measurements. It can be seen that spectral response of the optical filters are quite uniform across different pixel positions and hence we calculate the response of an filter as an average across the pixels corresponding to the filter (step 4 of QE measurement). In Figure 11, we show measurements of reflectance spectra of Erbium Oxide and green leaf using an imec hyperspectral sensor (same as in Figure 10). The reflectance spectra was measured at three different locations on the sensor (center, left and right). It can be seen that the measured spectra closely matches the reference spectra and also that the spectra measured in three different locations of the sensor closely matches.

In Figure 12 and Figure 13, we show the validity of the proposed pixel response model by comparing the reflectance spectra for two colors of Esser Chart obtained using the proposed model and through measurement. The measured data is the raw spectrum output of the camera without any reflectance and spectral correction applied.

DOI: 10.2352/ISSN.2470-1173.2016.12.IMSE-280

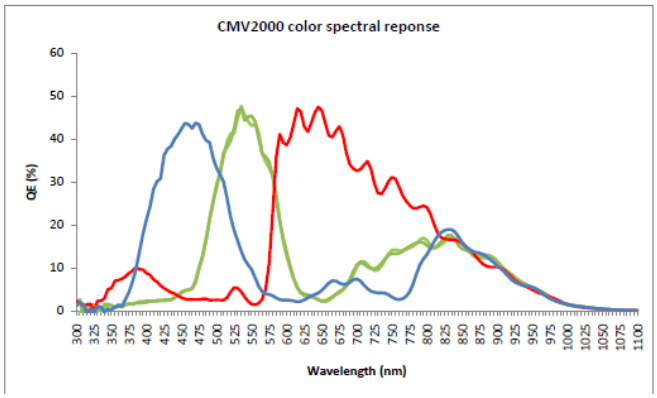

Figure 8 The QE of the RGB CMV2000 sensor as specified by CMOSIS

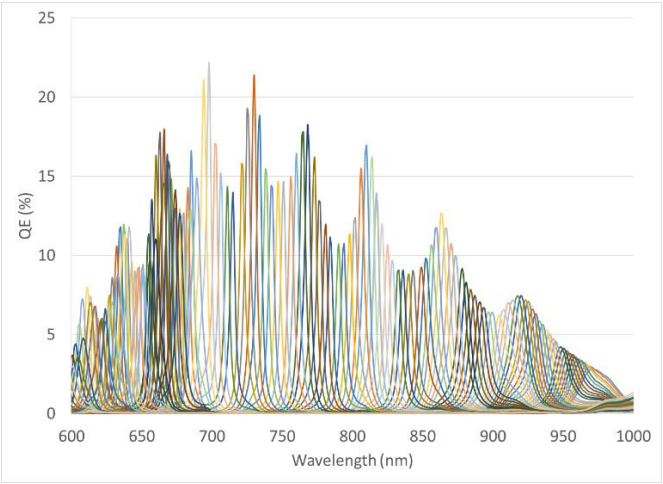

Figure 9 A typical measurement of the spectral response of an HSI sensor with 128 bands

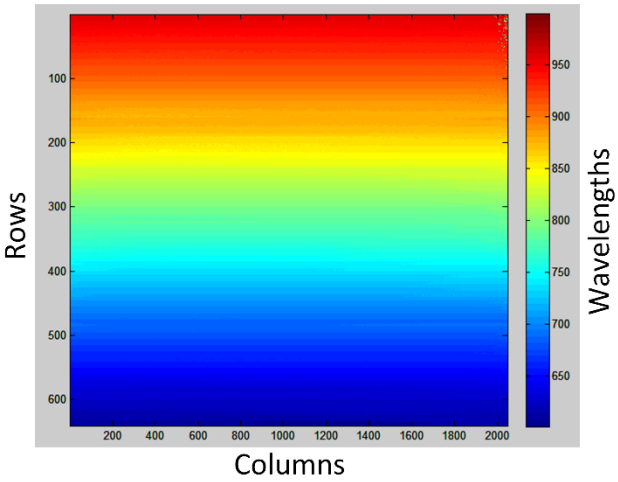

Figure 10 Measurement of central wavelength at each pixel position for an imec hyperspectral sensor with 100+ optical filters in linescan pattern

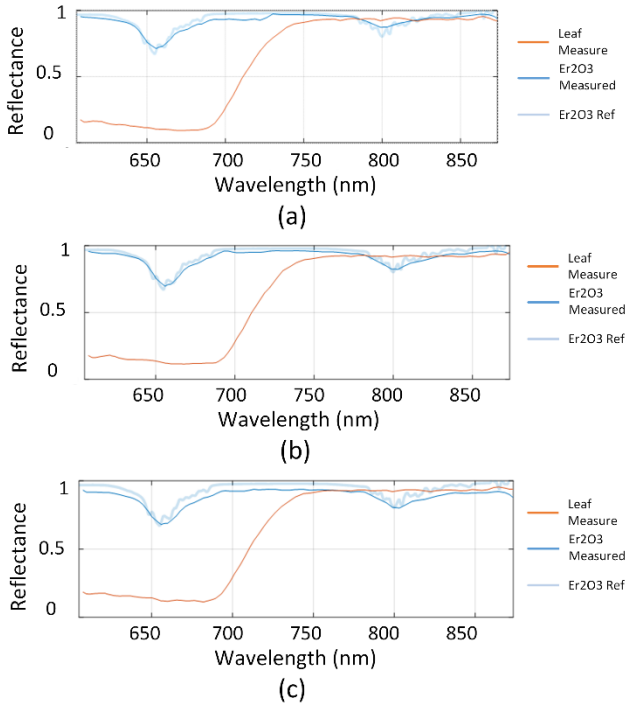

Figure 11 Measurement of reflectance spectra of Erbium Oxide and green leaf from three different locations of an imec hyperspectral sensor (same as in Figure 10) – (a) Center, (b) Left and (c) Right

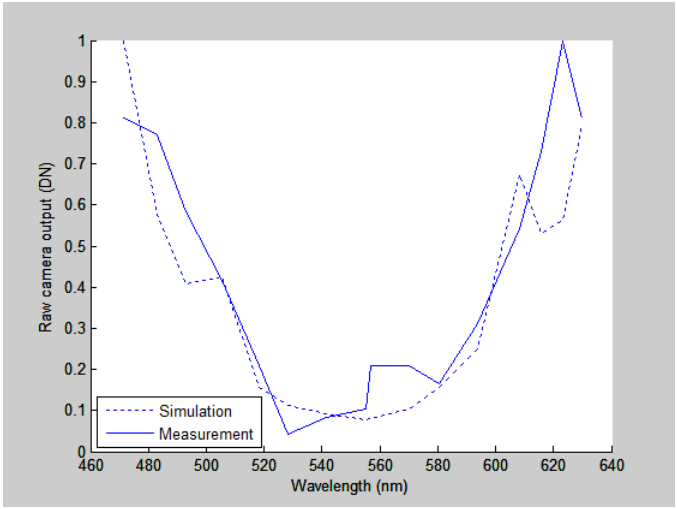

Figure 12 Comparison between measured and simulated response for blue color from Esser chart

©2016 Society for Imaging Science and Technology
DOI: 10.2352/ISSN.2470-1173.2016.12.IMSE-280

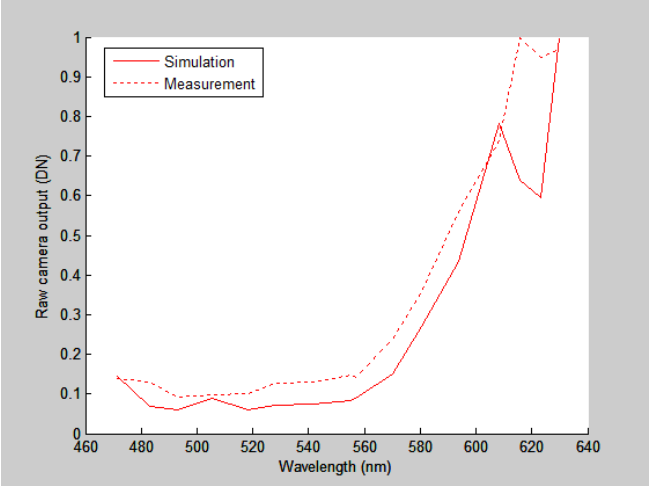

Figure 13 Comparison between measured and simulated response for red color from Esser chart

Noise Measurement

We use Photon-Transfer Curve (PTC) based approach to measure noise parameters, conversion gain, full-well capacity and dynamic range of the sensor. We use the method as specified in the EMVA Standard 1288 Rel 3.0 [6] for obtaining the PTC. The photo transfer method treats the sensor as a system block with light as the input and the digital data as the output. The difference in noise at the input and output can be assumed to have been introduced by the sensor. This method involves the measurement of mean values of the digital output and the temporal variance of these mean values at different irradiance levels. Different irradiance levels can be obtained either by varying intensity of the input light or by varying the integration time of the sensor using a constant illumination. In Figure 14, we show the photon-transfer curve obtained for the hyperspectral sensor, which is averaged across all the optical filters of the sensor. This sensor consists of 25 filters arranged in a mosaic 5x5 pattern. We also obtain PTC curve for each optical filter, as shown in Figure 15. We show that the optical filters do not impact the conversion gain and read noise for the sensor. However, the full well capacity measured across the optical filters can vary due to variation in the maximum digital signal measured across the filters (Figure 15).

Dark Current Measurement

As the dark current measurement is without using the light, the incidence angle dependency of the monolithically integrated optical filters can be ignored. Hence, we measure the dark current for these hyperspectral sensors using the standardized procedure as specified in EMVA Standard 1288 Rel 3.0 [6]. The method requires that mean of dark values at least six equally spaced exposure times are obtained. The dark current is the slope in the relation between the exposure times and the mean of the dark values [6]. In Figure 16, we compare the dark current measured for an imec hyperspectral sensor (with 100+ optical filters in a linescan pattern) and a panchromatic sensor without spectral filters. The hyperspectral sensor is based on such a panchromatic sensor. We show that the monolithic integration of filters does not degrade the dark current characteristics of the underlying CMOS image sensor. This has been tested and measured for other imec hyperspectral sensors also.

Conclusions

In this paper, we have presented the calibration procedures for imec hyperspectral sensors where Fabry-Perot interferometer based optical filters are monolithically integrated on standard CMOS image sensor. As these sensors are unique and first of its kind, the characterization procedures are not well defined and to the best of our knowledge they are not available in the current state of art. We have also presented a pixel response model for these hyperspectral sensors. This model is adapted from the traditional pixel response model to take into account the incidence angle dependency of the response of Fabry-Perot interferometers.

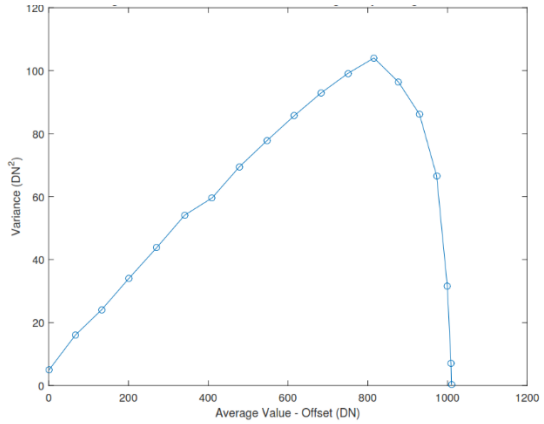

Figure 14 Photon-Transfer Curve for an imec hyperspectral sensor averaged across all the optical filters. The sensor consists of 25 filters arranged in a mosaic 5x5 pattern

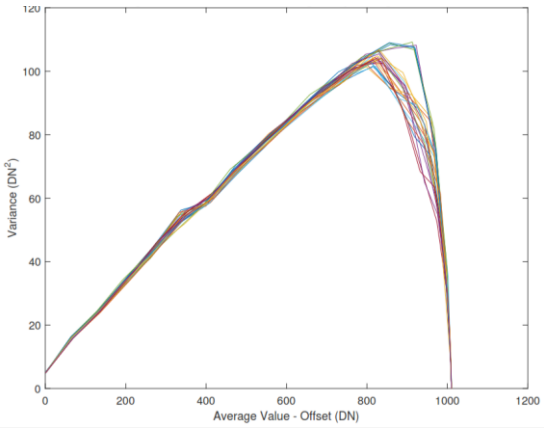

Figure 15 Photon-Transfer Curve for hyperspectral sensor (same Figure 14), obtained separately for each of the 25 optical filters

DOI: 10.2352/ISSN.2470-1173.2016.12.IMSE-280

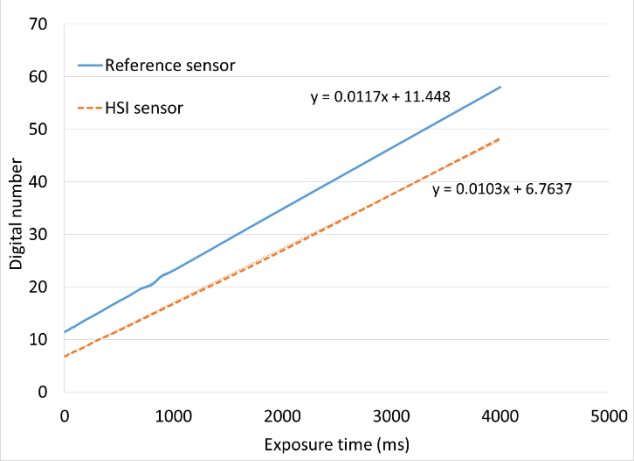

Figure 16 Comparison of dark current of panchromatic sensor (without any optical filters, referred to as reference sensor here) and HSI sensor (with 100+ optical filters in a linescan pattern)

Acknowledgements

This work was (partially) funded by the PHySIS project, contract no. 640174, within the H2020 Framework Program of the European Commission.

References

[1] N. Tack, A. Lambrechts, S. Soussan and L. Haspeslagh, "A compact, high-speed, and low-cost hyperspectral imager," in *Proc. SPIE 8266, Silicon Photonics VII*, 2012.

[2] B. Geelen, N. Tack and A. Lambrechts, "A compact snapshot multispectral imager with a monolithically integrated per-pixel filter mosaic," in *Proc. SPIE 8974, Advanced Fabrication Technologies for Micro/Nano Optics and Photonics VII*, 2014.

[3] B. Geelen, N. Tack and A. Lambrechts, "A snapshot multispectral imager with integrated tiled filters and optical duplication," in *Proc. SPIE 8613, Advanced Fabrication Technologies for Micro/Nano Optics and Photonics VI, 861314*, 2013.

[4] H. A. MacLeod, Thin-Film Optical Filters, Fourth Edition, CRC Press, 2010.

[5] P. L. Vora, J. E. Farrell, J. D. Tietz and D. H. Brainard, "Linear Models for Digital Cameras," in *50th Annual Conference: A Celebration of All Imaging*, 1997.

[6] "EMVA Standard 1288 Release 3.0".

Author Biography

Prashant Agrawal received his MS in Computer Science & Engineering from the Indian Institute of Technology Kharagpur (2009) and his PhD in Electrical Engineering from University of Leuven, Belgium (2015). He has been working in the Integrated Imaging Group at Imec in Belgium since 2014. He is working in hyperspectral imaging on sensor calibration procedures and exploring novel applications of hyperspectral imaging.

Klaas Tack received the engineering degree and a Ph.D. in electrical engineering from the Katholieke Universiteit Leuven, Belgium in 2001 and 2006 respectively. He is a Principal Engineer in the Integrated Imaging team at imec, His research interests currently focus on the development of novel hyperspectral imaging systems.

Bert Geelen received the engineering degree and a Ph.D. in electrical engineering from the Katholieke Universiteit Leuven, Belgium in 2003 and 2008 respectively. His research interests include optics, hyperspectral imaging system design and signal processing, low-power embedded-systems design and computer architectures. He is a member of the CMORES (CMORE Systems) Integrated Imaging group at the Inter-University Microelectronics Center (IMEC).

Bart Masschelein received his degree in Industrial Engineering from the KHBO (Belgium) in '98, after which he took an MSc-course in Electronic System Design, in collaboration with Leeds Metropolitan University. In '98, he joined the Multi-Media group at imec, Belgium and has been working in the field of still image and video compression, 3DTV image processing and image processing algorithms for novel imaging systems. His current focus lies in the field of hyperspectral imaging targeted for imec's proprietary hyperspectral sensor.

Mateo Aranda graduated from a MSc in Applied Physics and Photonics from Delft University of Technology and Friedrich-Schiller-University Jena (2013). He started working as a development engineer on the field of fiber optics at TE Connectivity in The Netherlands and in 2015 he joined the Integrated Imaging Group at Imec in Belgium where he works on the calibration of hyperspectral sensors.

Andy Lambrechts received his MSE from the KULeuven (2003) and his PhD in Electronics from the same university and imec in 2009. Since then he has worked at imec, Belgium, on hyperspectral imaging. He is currently leading the Integrated Imaging team and has focused on novel imaging applications, e.g. Spectral imaging and lens-free microscopy.

Murali Jayapala obtained his MsEE in Systems Science and Automation from the IISc (in 1999) and his PhD in Applied Sciences from the University of Leuven, Belgium (in 2005). After his research on low-power embedded system design, he is now focusing on system design aspects for next generation imaging systems exploiting various semiconductor technologies including hyperspectral imaging, lensfree microscopy, micromirror based lenses, diffractive optics.